Solar RRL

WILEY VCH

Solar RRL

RESEARCH ARTICLE OPEN ACCESS

Photoluminescence Degradation in Metal Halide Perovskites: Is In-Situ Study with Concentrated Sunlight Possible?

Rafael Fleischman[1] | Max Grischek[2] | Jiahuan Zhang[2] | Florian Scheler[2] | Georgios E. Arnaoutakis[3] | Mark Khenkin[2] | Carolin Ulbrich[2] | Steve Albrecht[2] | Eugene A. Katz[1]

[1]Swiss Institute for Dryland Environmental and Energy Research, J. Blaustein Institutes for Desert Research, Ben-Gurion University of the Negev, Midreshet Ben-Gurion, Israel | [2]Solar Energy Division, Helmholtz-Zentrum Berlin für Materialien und Energie GmbH, Berlin, Germany | [3]Power Systems Synthesis Lab, Mechanical Engineering Department, Hellenic Mediterranean University, Heraklion, Greece

Correspondence: Eugene A. Katz (keugene@bgu.ac.il)

Received: 12 January 2025 | **Revised:** 28 March 2025 | **Accepted:** 31 March 2025

Funding: Ministry of Innovation, Science and Technology of Israel, Grant/Award Number: 8117261

Keywords: concentrated sunlight | degradation | metal halide perovskites | photoluminescence

ABSTRACT

Photoluminescence (PL) spectroscopy is a valuable tool fordegradation studies of perovskite-based photovoltaic materials. The wavelength-sensitive nature of the photo-induced processes implies a preference for sunlight as the photo-excitation source for such PL studies. This study reports on the design and experimental validation of a new setup for the in situ study of PL degradation in metal halide perovskites using concentrated natural sunlight in a wide range of solar concentrations and sample temperatures. The system allows the sample to be excited with the entire solar spectrum while successfully filtering undesired reflected sunlight using two orthogonal polarization filters. Depending on temperature and solar concentration, we observed three types of perovskite PL behavior: stable PL response, without degradation; reversible PL degradation with stable ultraviolet–visible light absorption; and nonreversible PL degradation accompanied with the variation of light absorption.

1 | Introduction

Since the first demonstration of applying metal halide perovskites (MHP) as a photovoltaic (PV) material in 2009 [1], solar cells based on these novel semiconductors have shown remarkable progress, achieving power conversion efficiency of up to 26.7% [2]. However, considerable improvement in the operational stability of these devices is needed for implementing this technology [3, 4]. Photoluminescence (PL) spectroscopy [5, 6] and imaging [7] are among the most powerful, potent, and widespread tools to support progress in this direction.

One of the specific features behind the behavior of MHP cells is the significance of slow (from seconds to hours) metastable and often reversible processes such as ion migration and trap generation/activation/deactivation. PL kinetics (i.e., the evolution of PL intensity under laser excitation on various—usually minutes—timescales) has been reported to study such processes [8, 9]. However, the details of the underlying processes and their connection to the structure of the perovskite material and fabrication remain unclear. Both PL enhancement and deterioration were observed in perovskites under light soaking [10]. Rising PL intensity has been associated with trap filling by photogenerated electrons that gradually reduces the availability of trap sites and hence nonradiative recombination [11, 12]. It has been further reported that the rise of PL is a combined effect of trap deactivation and reversible photogenerated carrier lateral diffusion [13]. This was also confirmed in perovskite devices [14]. In devices, each layer may enhance or reduce the PL intensity and, therefore, change the PL kinetics under the excitation light [9, 15, 16].

Although trap filling explains the PL rise over the initial few seconds, it cannot explain PL changes over minutes to hours. These were explained in terms of a photochemical reaction of defect sites that diffuse from the surface to the bulk of the crystal [17, 18], especially efficient in large crystals [19, 20] and further distinguished between photo bleaching and photo blinking [21]. Migration of iodide ions away from the illuminated area, confirmed via time-of-flight secondary ion mass spectrometry [22], has also been reported as an explanation of the PL rise over time. Using trap density calculations, Mosconi et al. [23] suggested that photo-induced annihilation of iodine Frenkel pairs may explain the change in PL.

PL is a valuable tool for MHP materials degradation studies in addition to commonly used ultraviolet–visible (UV–Vis) light absorption and structural methods. Although UV–Vis is an effective tool for screening the photo-induced decomposition of MHPs [24, 25], it does not capture earlier degradation effects, which only affect the material's electronic properties. PL, therefore, is a much more sensitive tool for monitoring MHP degradation at its initial stages [26]. It was also reported that the excitation wavelength has a significant effect on the observed degradation of perovskite [27, 28]. A long-term decaying PL was reported under UV excitation of $MAPbI_3$ films at 266 nm [29] as well as 405 nm [30] and 457 nm [28] illumination.

Concentrated sunlight has already been demonstrated as a powerful tool for accelerated studies of the intrinsic degradation of perovskite films [24–26, 31] and solar cells [32, 33]. The wavelength-sensitive nature of the photo-induced processes implies a preference for sunlight as the photo-excitation source for PL studies of MHP PV materials and devices in all three research avenues mentioned above: (a) short-term (seconds–minutes scale) transient processes and instabilities, (b) long-term degradation (including perovskite decomposition), and (c) probing dominant recombination mechanism(s). For these purposes, we have developed a novel experimental setup and research methodology for in situ PL monitoring under excitation by concentrated natural sunlight. The topic of the present paper is the description of this methodology and its application to the in situ study of the accelerated degradation of MHP thin films under concentrated sunlight.

2 | Results and Discussion

2.1 | Obtaining a Clear PL Signal

We have designed and realized a novel experimental setup in which PL is excited by concentrated sunlight. The setup is based on a "solar furnace" [24, 34–36] in which natural sunlight is transmitted indoors and concentrated by a parabolic aplanat dish (Figure 1). The main limitation of this experimental approach is overlapping the perovskite PL emission line with an intensive reflection of concentrated sunlight. In the first generation of the system, to avoid such overlapping, sunlight excitation with wavelength $\lambda > 690$ nm was filtered by dichroic and short-pass filters. Only sunlight with 340 nm $< \lambda <$ 690 nm was used for PL excitation. Figure 2a shows a typical normalized-PL spectrum of an encapsulated thin film of methylammonium lead iodide ($MAPbI_3$) under filtered sunlight excitation. The spectrum shape does not differ from that recorded under a laser excitation, which proves viability of the concept. However, part of the solar spectrum was filtered out from the excitation which slightly undermines the purpose of the setup.

To use the entire solar spectrum, the system was upgraded to a new version (Figure 3), which will be called the second generation throughout the manuscript. Two orthogonally oriented polarization

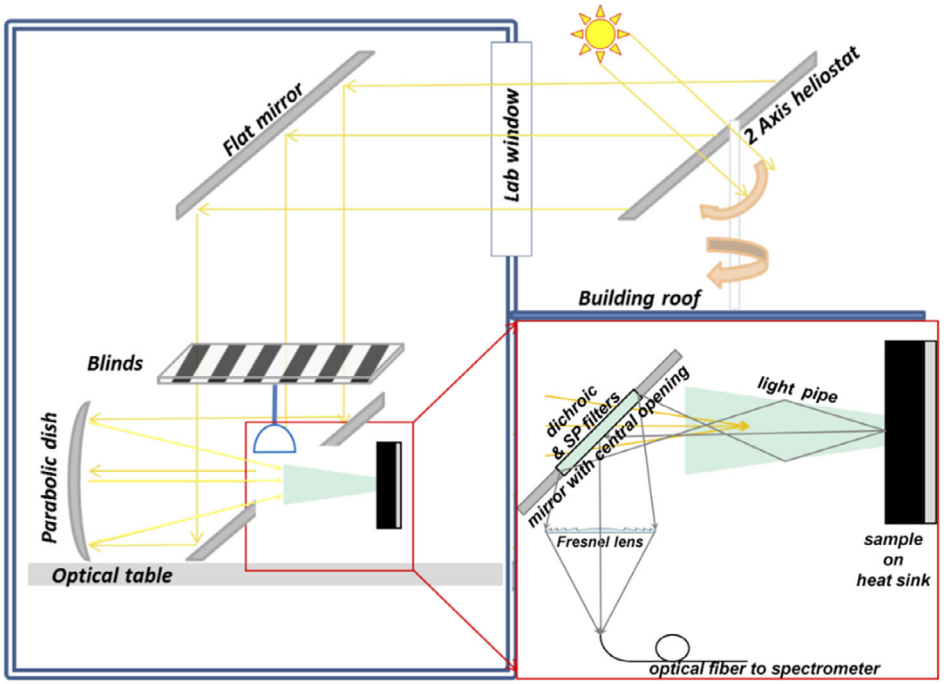

FIGURE 1 | Schematic of the experimental setup in which PL is excited by concentrated sunlight. A tracking system is used to provide sunlight in the lab area. The detail in the red frame shows the optical elements used for the excitation and collection of the PL of the MHP samples. MHP = metal halide perovskite; PL = photoluminescence.

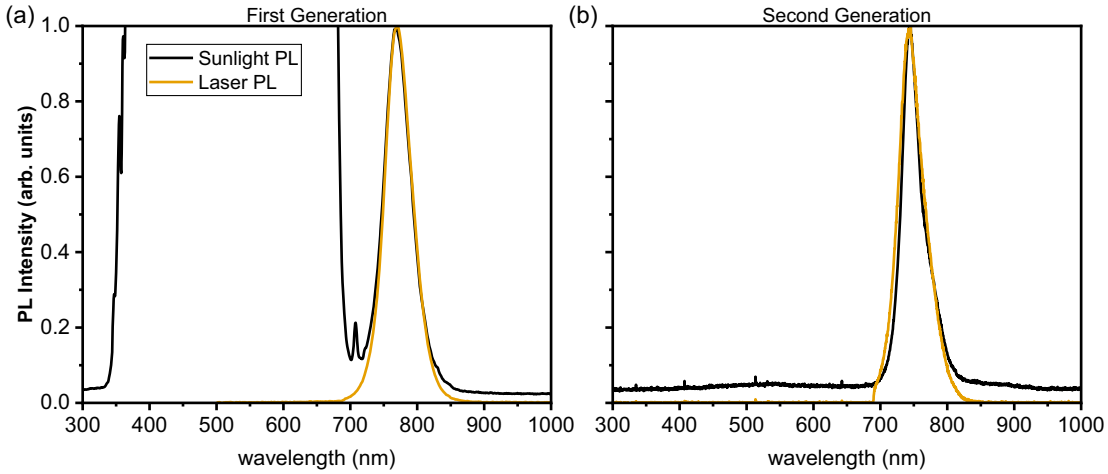

FIGURE 2 | Typical normalized PL spectra of MHP films excited by laser and sunlight. (a) A spectrum obtained using the first-generation system (where part of the solar spectrum was filtered by dichroic and short-pass filters), while (b) one using the second-generation system (where the whole solar spectrum is used and reflection is blocked using two orthogonally oriented polarization filters). Both approaches result in PL spectrum similar to the one recorded in the laboratory setup using laser excitation. MHP = metal halide perovskite; PL = photoluminescence.

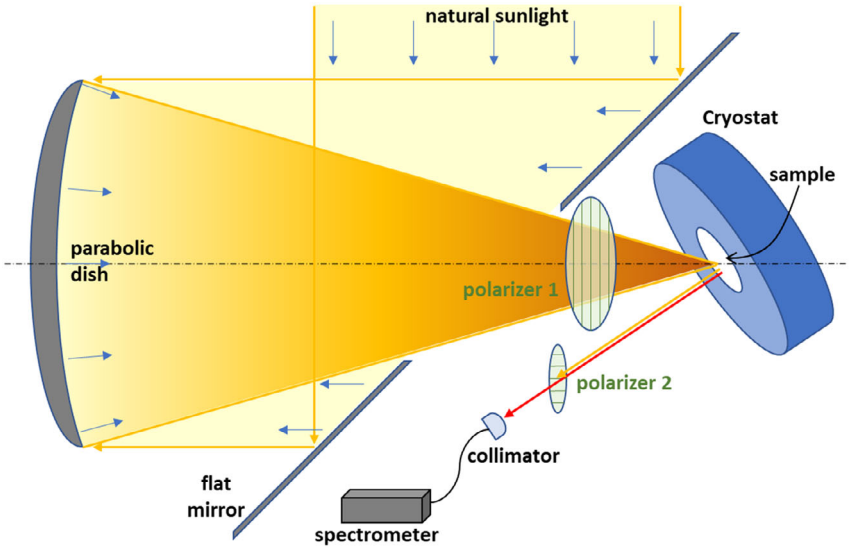

FIGURE 3 | Schematic of the second generation of the experimental configuration. PL is measured by a spectrometer, while reflected sunlight is blocked with a system of orthogonal polarization filters in respect to each other. The sample is placed inside a cryostat with temperature control. PL = photoluminescence.

filters were placed instead of filtering out part of the sunlight. The new system allows the undesired reflected sunlight to be blocked by up to three orders of magnitude in intensity (Figure S1, Supporting Information). The typical PL spectrum of the MHP film obtained with the new system is displayed in Figure 2b. Here and in all experiments described below, the perovskite formulation was $(FA_{0.22}Cs_{0.78}Pb\ (Br_{0.15}I_{0.85})_3$ + $MAPbCl_3)$, sometimes referred to as triple-halide [37]. The sample preparation and their layered sequence are described in the Experimental Section.

2.2 | Independent Control of Light Intensity and the Sample Temperature

The system allows variation and control of the incident intensity of concentrated sunlight (P_{in}) by adjusting the opening of the blinds between the two flat mirrors (Figure 1). For the complete open blinds, the sample is illuminated by *Pin* up to 8000 suns. To control the sample temperature (T) independently from the P_{in}, the sample is placed inside a liquid nitrogen cryostat (Figure 3). Throughout this article, 'light intensity' refers to the insolation reaching the sample.

Figure 4 shows an example of the variation of the PL peak intensity and PL spectra of the MHP film kept at $T \sim 80$ K and exposed to various P_{in} (from 7 to 42 suns). PL peak intensity was found to increase with P_{in} increase within this intensity range.

One initial concern was that the actual temperature inside the encapsulated sample might become higher than its measured value due to exposure to the high light intensity, since heat removal in the cryostat is performed around the sample,

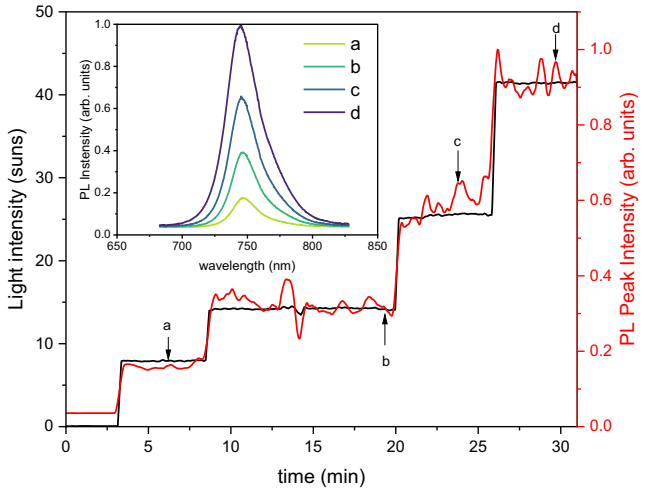

FIGURE 4 | peak intensity of an MHP film at the constant temperature of about 80 K (with adjacent averaging smoothing with 20 points). P_{in} was increased in steps to 1, 8, 14, 26, and 42 suns. For each step, one representative point was selected (points a–d), and its PL spectrum is presented in the inset graph. MHP = metal halide perovskite; PL = photoluminescence.

and the temperature sensor is located behind it (opposite to the illuminated surface of the sample). Figure 5 provides unambiguous evidence of the constant temperature of the sample illuminated by various solar concentrations. In this case, we consider the PL peak energy position/MHP bandgap as an additional measure of the cell temperature. Although the MHP bandgap would increase with the temperature [38, 39], neither the measured T (on the back of the sample) nor the PL peak position was affected by the increasing P_{in} throughout the measurement. This indicates that the light intensity and the sample temperature can be varied independently in the designed setup.

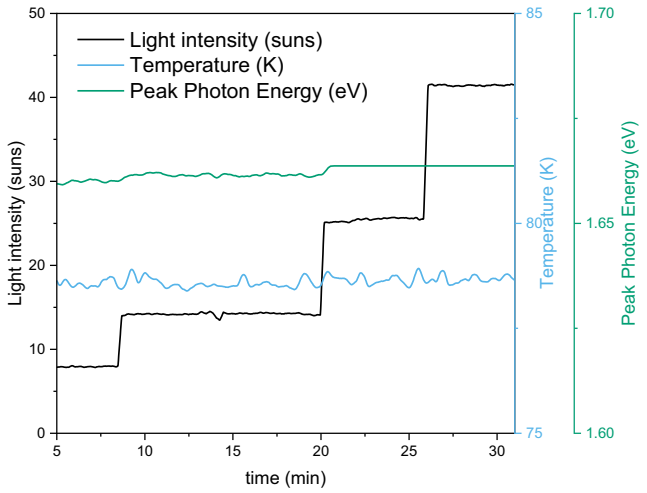

FIGURE 5 | P_{in} (black), temperature (blue), and PL peak photon energy (green) of the sample during the experiment. Although the P_{in} was increased in steps from 8 to 42 suns, both the measured temperature and the PL peak photon energy remained constant, indicating that the sample did not heat up. Adjacent averaging smoothing with 20 points was used on the temperature and peak photon energy series. PL = photoluminescence.

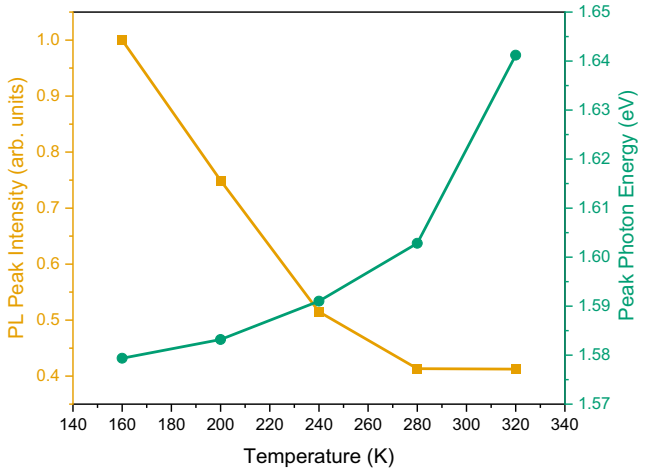

FIGURE 6 | PL peak intensity (normalized to the value at 160 K) as yellow squares and PL peak photon energy as green circles as a function of temperature under illumination of constant intensity of 26 suns. PL = photoluminescence.

Figure 6 depicts the results of the experiment in which the sample was exposed to constant P_{in} (26 suns in this case) at different temperatures (from 320 to 160 K). Each exposure lasted for ~10 min. There were dark intervals of 10 min between the illumination periods when the temperature was stabilized at the new level. The PL signal stayed stable throughout every illuminated period. As expected, the PL peak exhibited a blue shift with increasing temperature, indicating an increase in the material bandgap with temperature [38, 40], while PL peak intensity decreased with temperature due to the known thermal activation of nonradiative recombination mechanisms [41–43].

2.3 | Reversible PL Degradation

In the experiments described above (Figure 4–6), the PL signal was reasonably stable during the measurement. However, after reaching certain thresholds in P_{in}, a degradation in PL can be observed. In the scope of this work, we define PL degradation as a gradual decrease in the PL intensity during the illumination time. The threshold values of P_{in} for the onset of PL degradation start can also depend on the sample temperature. This dependence will be discussed below.

Figure 7a illustrates an experiment in which considerable PL degradation was observed already at P_{in} ~ 15 suns. PL peak intensity decreased to around 45% of its initial value. Immediately after the experiment ended (point f in Figure 7a), the UV–Vis light absorption spectrum of the sample was measured (see Figure 7b). The absorption spectrum did not differ significantly from that measured for this sample before the PL experiment started. This result suggests that: (1) there is no perovskite photodecomposition previously observed under highly concentrated sunlight [25] (see also Section 2.4 below) and (2) PL degradation originates from the generation of centers of nonradiative recombination.

Previously, we observed that PL degradation can be reversible: PL was found to restore in the absence of illumination [26]. A set of

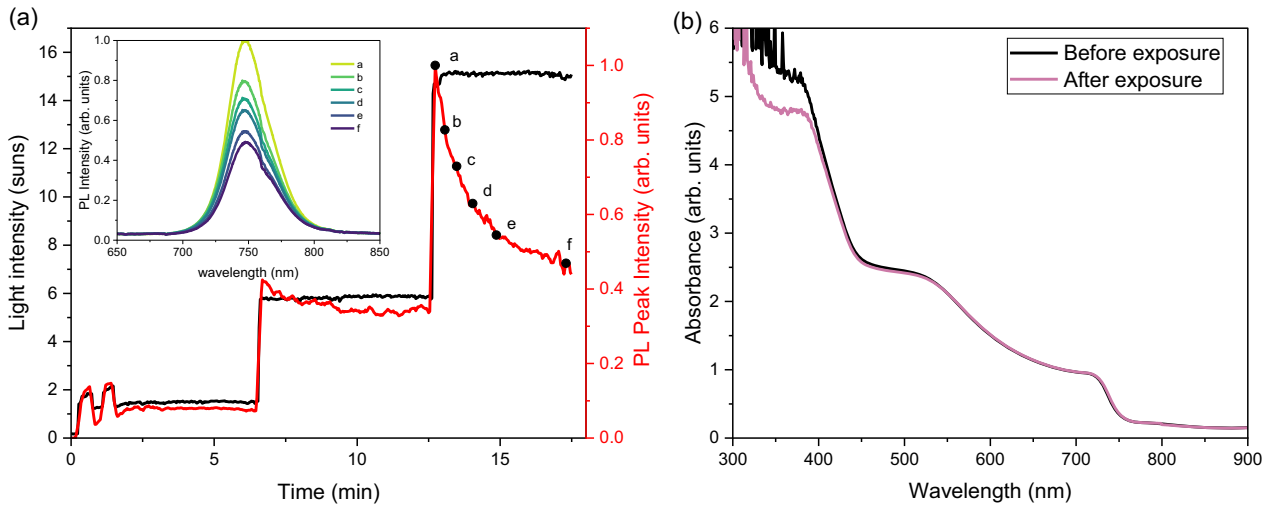

FIGURE 7 | (a) PL of a MHP film exposed to increasing light intensities at $T = 210$ K. The inset presents PL spectra during the degradation phase and (b) the UV–Vis light absorption spectrum of the sample taken before and after the PL experiment. Adjacent averaging smoothing with 5 points was used on the PL peak intensity series. MHP = metal halide perovskite; PL = photoluminescence; UV–Vis = ultraviolet–visible.

further experiments was performed to study this behavior. In these experiments, the perovskite samples were (1) exposed to a combination of incident light and temperature until the PL degradation was noticed, (2) then allowed to regenerate in the absence of light, and (3) finally, the samples were brought back to the same illumination conditions.

Figure 8 presents one such experiment. Following the procedure described in Figure 7, the sample was allowed to recover in the dark at room temperature for 3 days. Then, it was re-exposed to light for the second time, and PL intensity reached high levels, indicating that some regeneration took place during the dark period. Also, the initial PL of the second curve is significantly higher than that of the first curve (PL peak intensity reached a level of 230% compared to the first exposure). This is due to the initial pre-exposure to 5 suns and was experienced only in the first exposure. Following this, the sample recovered in the dark for 5 min and then subsequently exposed to sunlight for the third time. The short rest allowed for limited recovery only: PL peaked at 70% of its initial value. The same light intensity of 15 suns and temperature of 210 K was used in all three exposures. Interestingly, despite the initial PL intensities of each exposure, in all cases, PL quickly degraded and stabilized at around the same level of 50% of its initial value after about 4 min. All the values were normalized in relation to the PL peak of the first exposure.

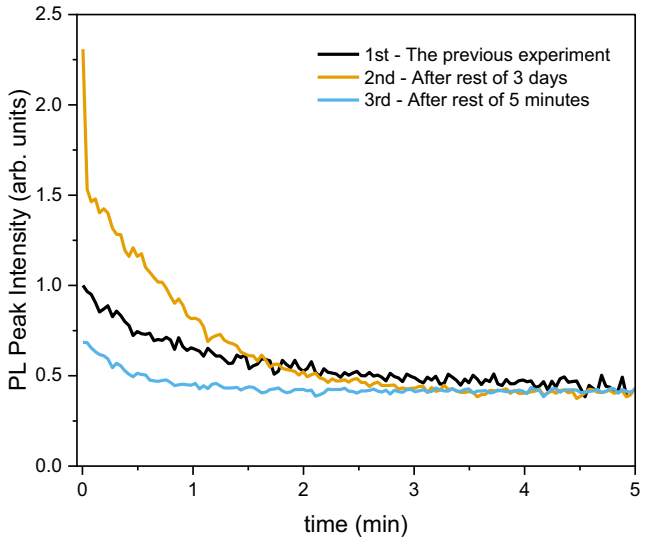

FIGURE 8 | MHP film PL intensity of three consecutive exposures to $P_{in} = 15$ suns and $T = 210$ K. The first one is the last part of the experiment presented in Figure 7 and has been pre-exposed to 5 suns. The second exposure was obtained after a rest period of 3 days in the dark, which allowed for a complete recovery. The third one was obtained after an additional 5 min rest period after the second, resulting in partial recovery only. The PL peak intensity values are normalized with respect to the maximum value of the first exposure. MHP = metal halide perovskite; PL = photoluminescence.

Additional experiments were performed, where, depending on the time of the dark period, partial or complete PL recovery was recorded. Figure S2, Supporting Information illustrates the reversible PL degradation of a sample kept at 120 K and alternatively exposed to 40 suns and dark, where after short intervals of light exposure, the PL intensity converges to the same level, independent of the sample recovery status.

The in situ PL approach allows tracing dynamic transient effects in perovskite materials (which are affected by the measurements and storage history), contrary to when degradation and PL measurements occur in different experimental setups.

Possible underlying mechanisms of reversible photo-induced changes in MHP PL are widely discussed in the literature [44–47]. They include ion migration, formation of interstitial defects of iodine and lead, as well as generation of other bulk and surface traps and centers of nonradiative recombination, including those formed at the grain boundaries' vicinity. The degree of reversibility depends on the perovskite environment [45], the grain size [46], and the intensity of the excitation laser light [47]. Surface trap states can promote long-range ion migration and charge

accumulation, while bulk trap states are primarily responsible for mobile ionic defects [48]. PL changes governed by the photoinduced halide phase segregation can also exhibit the reversible character [49]. In our case, this mechanism can be excluded since, in the above-described experiments, we did not observe the evolution of the PL peak shape and energy position that are characteristic of the halide phase segregation [50–52].

2.4 | Nonreversible PL Degradation

Further increasing the illumination intensity was observed to shift reversible degradation pathways to nonreversible ones.

Figure 9 shows a characteristic result of PL degradation under high illumination intensities. A sample was brought to 120 K and exposed to ~30 suns while continuously measuring the sample PL. After some minutes, the P_{in} was rapidly increased to ~120 suns. As a result, the PL signal immediately increased and then quickly degraded in less than a minute, reaching about 25% of the initial PL peak intensity value.

It should also be noted that the PL spectra measured at the final stages of the degradation (points b, c, and d in Figure 9) show a changed shape with the appearance of the second peak shifted to a higher wavelength (low photon energy). This can be explained by phase halide segregation and the formation of iodide-reached domains with lower bandgap, the so-called Hoke effect [49].

If the experiment was interrupted after 30 s of illumination by 120 suns (the time of the most PL decline shown in Figure 9), the UV–Vis absorbance spectra before and after illumination were not substantially different (Figure S3a, Supporting Information). This difference was increased after the prolonged experiment (Figure S3b, Supporting Information).

After such exposure, the PL signal of this sample was never restored to the initial value, even after resting in the dark for 8 days. This makes our findings different from the reversible Hoke effect observed previously [49–52]. This may be explained by a difference between our 'white' solar excitation and the monochromatic laser excitation used in the Hoke effect experiments. Indeed, it has been shown, for example, that the kinetics of the phase halide segregation varies with the energy of the excitation source [53].

2.5 | PL Degradation Threshold Dependence on Sunlight Intensity and Temperature

As discussed previously, the outcome of PL degradation depends on both the temperature and the light intensity. Figure 10 summarizes the experimental outcome of 90 experiments performed during the study. Indeed, higher temperatures and light intensities favored the PL degradation. Finding the specific dependence of the PL degradation threshold on the incident illumination intensity and the sample temperature was beyond the scope of the present study and may strongly depend on perovskite formulation and sample preparation conditions. However, a general pattern hints at the decrease of the light intensity threshold with increasing sample temperature.

3 | Summary and Outlook

We designed, built, and experimentally validated a new, unique setup for the in situ study of PL degradation in MHPs using concentrated natural sunlight. The setup can independently vary sunlight concentration and sample temperature in a broad range. The system allows the sample to be excited with the sunlight of a natural spectrum while successfully filtering undesired reflected sunlight (up to three orders of magnitude) using two orthogonal polarization filters. We demonstrated the capability of the setup to (1) characterize perovskite PL without damaging the material (low T and/or Irradiance), (2) study transient effects during the light and dark periods, and (3) trace the accelerated degradation under high irradiance illumination resulting in the perovskite decomposition. The designed setup unlocks the possibility of mapping the dependence of the PL degradation threshold on

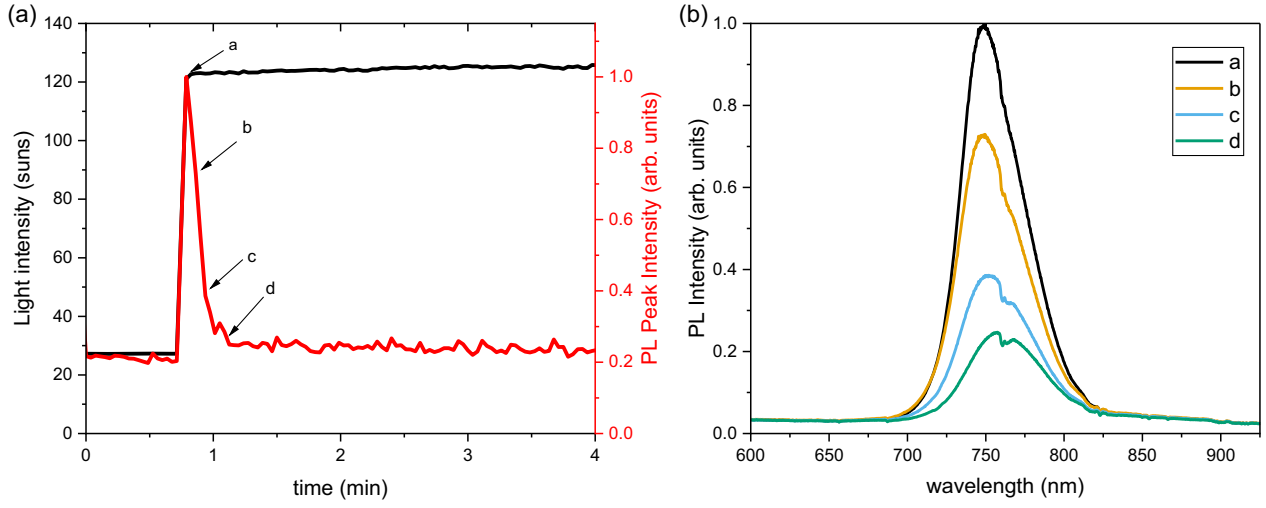

FIGURE 9 | Nonreversible degradation of MHP film under $P_{in} = 120$ suns and $T = 120$ K. (a) The fast decrease in PL peak intensity following exposure to high P_{in} and (b) some selected spectra during the fast degradation phase. MHP = metal halide perovskite; PL = photoluminescence.

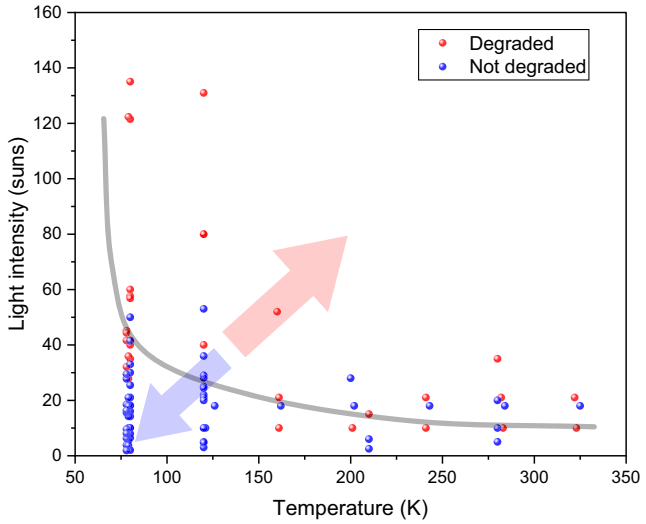

FIGURE 10 | Experimental outcome on degradation of multiple perovskite samples under a wide range of temperatures and light intensities. An increase in both temperature and light intensity leads to a higher chance of PL degradation. The gray line is for eye guidance only. PL = photoluminescence.

the incident illumination intensity and the sample temperature for a variety of perovskite materials.

While PL degradation may strongly depend on perovskite formulation and sample preparation conditions, it is undoubtedly accelerated by higher temperatures and light intensities. Increase in the sample temperature can decrease the light intensity threshold of PL degradation. Additional research, with a rigorous methodology for sample preparation/characterization and a clear definition of PL degradation, is required to accurately map the dependence of the PL degradation threshold on the incident illumination intensity and the sample temperature.

Our future studies will also include extending the range of perovskite materials as well as perovskite solar cells. In the latter case, we are going to connect the accelerated degradation of perovskite PL with the corresponding changes in PV performance. We will also use an approach of voltage-dependent PL in an operating solar cell [54, 55] that was recently proposed to identify the radiative and nonradiative losses and investigate the loss mechanisms. PL-based imaging could spatially resolve electrical parameters and provide insights into recombination mechanisms [56], including carrier collection losses [57].

4 | Experimental

Experiments in our lab target the study of PL of perovskite samples excited by natural sunlight. The setup is based on a "Solar Furnace" (Figure 1) concentrating system [24, 34–36] in which natural concentrated sunlight is transmitted indoors and concentrated through a parabolic aplanat concentrating system, described in detail elsewhere [34].

A 2-axis heliostat is used to track the sun. It is moved by a stepper motor, and often, even slight misalignments caused by the motor action result in periodic oscillations in the intensity of the measured PL, as is evident in many of the presented results.

4.1 | First-Generation System Characterization

In the first-generation configuration, sunlight excitation was filtered by an array of short wave-pass dichroic filters (Edmund optics, 69–217, 650 nm) and a 4 x 4 IR-absorbing filter (Edmund optics KG-1, 700 nm) so that sunlight between 340 nm $< \lambda <$ 690 nm was used for excitation.

The PL was collected through a homogenizing truncated square pyramidal light pipe and reflected to a single slit optical fiber UV–Vis spectrometer (Avantes, ULS2040CL) through a 10 x 10 cm Fresnel lens. The samples were mounted on a 75 x 60 x 50 mm aluminum heat sink. The temperature of the films, monitored by thermocouples, was kept within 25 ± 3°C during the experiments. The temperature stability was independently confirmed by photo-luminescent thermometry presented elsewhere [36, 58].

4.2 | Second-Generation System Characterization

The second-generation system is based on the previous one (Figure 3), but instead of filtering out part of the sunlight, a system of polarization filters (Wire Grid Versalight by Meadowlark) placed orthogonally in respect to each other to block the undesired reflected sunlight. The sample is placed in a cryostatic chamber (Oxford Instruments Microstat) with a Mercury iTC controller (80–500 K range). The PL was collected through a collimator and directed by a single slit optical fiber, carefully aligned, to a UV–Vis spectrometer (Avantes, ULS2040CL).

A continuous flow nitrogen cryostat chamber (Oxford Instruments MicrostatN) is used for temperature control, with a temperature range from 77 to 500 K. The sample is mounted in a vacuum on a copper heat exchanger and cooled by conduction. The sample chamber is pumped continuously with a two-stage rotary pump, while the cryostat is running. Optical access is available through a window. The liquid nitrogen flows through the heat exchanger at the bottom of the sample space, through the sample space, and out of the cryostat to the pump. A thermometer and heater are mounted on the heat exchanger, and these are used with a Mercury iTC temperature controller to balance the cooling power of the cryogen and to control the temperature of the gas before it reaches the sample space.

4.3 | Metal Halide Perovskite Film Deposition

Glass/indium tin oxide substrates were cleaned in sonicating bath, using H_2O + soap, H_2O, acetone and isopropyl alcohol. All following steps were conducted inside inert nitrogen atmosphere. For the hole transport layer, 3 mmol/l 2PACz dissolved in ethanol was spin-coated at 3000 rpm for 20 s, following annealing at 100°C for 5 min.

The wide bandgap 'triple-halide' perovskite composition was adapted due to its high V_{OC} potential in silicon-perovskite

tandem solar cells together with high phase stability [37]. First, a 1.4 M 'FACs' solution (FA, Cs, PbI_2, $PbBr_2$; 22% Cs & 15% Br) in 4:1 dimethylformamide: dimethyl sulfoxide was shaken at room temperature overnight. Next, it was transferred into another vial that contained MACl and $PbCl_2$ powders and shaken for 1 h at 60°C before perovskite layer deposition, with a nominal molar Cl percentage of 5%. Exemplary amounts of chemicals for 1 ml of 1.4 M solution: 500 mg PbI_2, 116 mg, $PbBr_2$, 188 mg FAI, 80 mg CsI (weighed into one vial) + 4.7 mg MACl, and 19.5 mg $PbCl_2$ (in another vial). The precursor solution was spin-coated at 5000 rpm for 50 s (5 s acceleration). At 25 s after the start of the process, 300 µL anisole as the antisolvent was applied. Finally, the films were annealed at 100°C for 20 min. The films were encapsulated using cover glasses and BLUFIXX SMART REPAIR UV-cured glue outside of the measured area.

4.4 | Sunlight Characterization

The solar PL experiments were performed at Sede Boqer (Desert Negev, Lat. 30.8°N, Lon. 34.8°E, Alt.475m) during clear-sky periods around noontime, when the solar spectrum is very close to the standard AM10.5 solar spectrum [59].

A system of blinds is used to control the incoming light intensity, allowing light intensities in the focus spot from 0 (blinds completely closed) to 8000 suns (blinds completely open). When the blinds are completely closed, the sample is subjected to negligible light intensities (in the order 10^{-3} suns), as only diffuse ambient light from inside the laboratory can reach it.

The incident light power on the sample was calibrated with a thermal power-meter (Ophir, FL250A) placed at the focal point of the parabolical dish (instead of the examined perovskite samples) and was controlled for real measurements with another thermal power-meter- meter (Thorlabs, S425C).

4.5 | UV–Vis Absorption

UV–Vis absorption experiments were performed with a UV–Vis and near-infrared spectrophotometer in the 175–3300 nm range (Agilent Technologies, Cary 5000). For experiments where the sample was exposed to repeated illumination sessions, the UV–Vis absorption experiments were performed immediately before and after placing the sample in the cryostat.

Acknowledgements

This research is partially supported by the Ministry of Innovation, Science and Technology of Israel in the framework of binational Israel – Italy scientific cooperation (project #8117261). R.F. thanks the Albert Katz International School for Desert Studies and the Kreitman School of Advanced Graduate Studies for the Negev PhD Fellowship program. M.G., J.Z., F.S. and S.A. acknowledge the Helmholtz project "Zeitenwende - Zukunftstechnologie Tandem Solarzellen." M.G. and S.A. acknowledge funding from the Helmholtz Association via HI-SCORE (Helmholtz International Research School). The authors thank J. Beckedahl, C. Ferber, M. Wittig, T. Lußky, and H. Heinz for the technical support in HySPRINT Helmholtz Innovation Lab.

Conflict of Interest

The authors declare no conflict of interest.

Data Availability Statement

The data that support the findings of this study are available from the corresponding author upon reasonable request.

References

1. A. Kojima, K. Teshima, Y. Shirai, and T. Miyasaka, "Organometal Halide Perovskites as Visible-Light Sensitizers for Photovoltaic Cells," *Journal of the American Chemical Society* 131, no. 17 (2009): 6050–6051, https://doi.org/10.1021/JA809598R.

2. *Best Research-Cell Efficiency Chart | Photovoltaic Research | NREL*2024, accessed December 02, 2024, https://www.nrel.gov/pv/cell-efficiency.html.

3. Perovskites Take Steps to Industrialization, *Nature Energy*, 5, no. 1 (2020): 1–1, https://doi.org/10.1038/s41560-020-0552-6.

4. M. V. Khenkin, E. A. Katz, A. Abate, et al., "Consensus Statement for Stability Assessment and Reporting for Perovskite Photovoltaics Based on ISOS Procedures," *Nature Energy* 5, no. 1 (2020): 35–49, https://doi.org/10.1038/s41560-019-0529-5.

5. T. Kirchartz, J. A. Márquez, M. Stolterfoht, and T. Unold, "Photoluminescence-Based Characterization of Halide Perovskites for Photovoltaics," *Advanced Energy Materials* 10 (2020): 1904134, https://doi.org/10.1002/aenm.201904134.

6. W. H. M. Remmerswaal, B. T. van Gorkom, D. Zhang, M. M. Wienk, and R. A. J. Janssen, "Quantifying Non-Radiative Recombination in Passivated Wide-Bandgap Metal Halide Perovskites Using Absolute Photoluminescence Spectroscopy," *Advanced Energy Materials* 14, no. 12 (2024): 2303664, https://doi.org/10.1002/aenm.202303664.

7. A. D. Bui, D.-T. Nguyen, A. Fell, et al., "Spatially Resolved Power Conversion Efficiency for Perovskite Solar Cells via Bias-Dependent Photoluminescence Imaging," *Cell Reports Physical Science* 4, no. 11 (2023), https://doi.org/10.1016/j.xcrp.2023.101641.

8. R. Brenes, D. Guo, A. Osherov, et al., "Metal Halide Perovskite Polycrystalline Films Exhibiting Properties of Single Crystals," *Joule* 1 (2017): 155–167, https://doi.org/10.1016/j.joule.2017.08.006.

9. N. S. Mahon, O. V. Korolik, M. V. Khenkin, et al., "Photoluminescence Kinetics for Monitoring Photoinduced Processes in Perovskite Solar Cells," *Solar Energy* 195 (2020): 114–120, https://doi.org/10.1016/J.SOLENER.2019.11.050.

10. S. D. Stranks, "Nonradiative Losses in Metal Halide Perovskites," *ACS Energy Letters* 2, no. 7 (2017): 1515–1525, https://doi.org/10.1021/ACSENERGYLETT.7B00239/ASSET/IMAGES/LARGE/NZ-2017-00239H_0004.JPEG.

11. S. D. Stranks, V. M. Burlakov, T. Leijtens, J. M. Ball, A. Goriely, and H. J. Snaith, "Recombination Kinetics in Organic-Inorganic Perovskites: Excitons, Free Charge, and Subgap States," *Physical Review Applied* 2 (2014): 034007, https://doi.org/10.1103/PhysRevApplied.2.034007.

12. Y. Yamada, M. Endo, A. Wakamiya, and Y. Kanemitsu, "Spontaneous Defect Annihilation in CH3NH3PbI3 Thin Films at Room Temperature Revealed by Time-Resolved Photoluminescence Spectroscopy," *Journal of Physical Chemistry Letters* 6, no. 3 (2015): 482–486, https://doi.org/10.1021/JZ5026596/ASSET/IMAGES/LARGE/JZ-2014-026596_0006.JPEG.

13. X. Fu, D. A. Jacobs, F. J. Beck, et al., "Photoluminescence study of time- and spatial-dependent light induced trap de-activation in $CH_3NH_3PbI_3$ perovskite films," *Physical Chemistry Chemical Physics* 18, no. 32 (2016): 22557–22564, https://doi.org/10.1039/C6CP03779H.

14. Y. Zhong, C. A. M. Luna, R. Hildner, C. Li, and S. Huettner, "In Situ Investigation of Light Soaking in Organolead Halide Perovskite Films,"

APL Materials 7, no. 4 (2019): 17, https://doi.org/10.1063/1.5086125/1024062.

15. X. Deng, X. Wen, J. Zheng, et al., "Dynamic Study of the Light Soaking Effect on Perovskite Solar Cells by in-Situ Photoluminescence Microscopy," *Nano Energy* 46 (2018): 356–364, https://doi.org/10.1016/J.NANOEN.2018.02.024.

16. J. Hu, L. Gouda, A. Kama, S. Tirosh, and R. Gottesman, "Radiative Recombination Changes under Light-Soaking in $CsPbBr_3$ Films on TiO_2 and Insulating Glass Contacts: Interface versus Bulk Effects," *ACS Applid Energy Materials* 2, no. 5 (2019): 3013–3016, https://doi.org/10.1021/ACSAEM.9B00335/ASSET/IMAGES/LARGE/AE-2019-003359_0002.JPEG.

17. Y. Tian, M. Peter, E. Unger, et al., "Mechanistic Insights into Perovskite Photoluminescence Enhancement: Light Curing with Oxygen Can Boost Yield Thousandfold," *Physical Chemistry Chemical Physics* 17, no. 38 (2015): 24978–24987, https://doi.org/10.1039/C5CP04410C.

18. M. Anaya, J. F. Galisteo-López, M. E. Calvo, J. P. Espinós, and H. Míguez, "Origin of Light-Induced Photophysical Effects in Organic Metal Halide Perovskites in the Presence of Oxygen," *Journal of Physical Chemistry Letters* 9, no. 14 (2018): 3891–3896, https://doi.org/10.1021/ACS.JPCLETT.8B01830/ASSET/IMAGES/LARGE/JZ-2018-01830B_0003.JPEG.

19. A. Merdasa, M. Bag, Y. Tian, E. Källman, A. Dobrovolsky, and I. G. Scheblykin, "Super-Resolution Luminescence Microspectroscopy Reveals the Mechanism of Photoinduced Degradation in $CH_3NH_3PbI_3$ Perovskite Nanocrystals," *Journal of Physical Chemistry C* 120, no. 19 (2016): 10711–10719, https://doi.org/10.1021/ACS.JPCC.6B03512/SUPPL_FILE/JP6B03512_SI_003.MPG.

20. A. Merdasa, Y. Tian, R. Camacho et al., "Supertrap' at Work: Extremely Efficient Nonradiative Recombination Channels in $MAPbI_3$ Perovskites Revealed by Luminescence Super-Resolution Imaging and Spectroscopy," *ACS Nano* 11, no. 6 (2017): 5391–5404, https://doi.org/10.1021/ACSNANO.6B07407/SUPPL_FILE/NN6B07407_SI_003.AVI.

21. L. Chouhan, S. Ghimire, and V. Biju, "Blinking Beats Bleaching: The Control of Superoxide Generation by Photo-Ionized Perovskite Nanocrystals," *Angewandte Chemie* 131, no. 15 (2019): 4929–4933, https://doi.org/10.1002/ANGE.201900061.

22. D. W. deQuilettes, W. Zhang, V. M. Burlakov, et al., "Photo-Induced Halide Redistribution in Organic-Inorganic Perovskite Films," *Nature Communications* 7, no. 1 (2016): 1–9, https://doi.org/10.1038/ncomms11683.

23. E. Mosconi, D. Meggiolaro, H. J. Snaith, S. D. Stranks, and F. De Angelis, "Light-Induced Annihilation of Frenkel Defects in Organo-Lead Halide Perovskites," *Energy & Environmental Science* 9, no. 10 (2016): 3180–3187, https://doi.org/10.1039/C6EE01504B.

24. E. A. Katz, I. Visoly-Fisher, D. Feuermann, R. Tenne, and J. M. Gordon, "Concentrated Sunlight for Materials Synthesis and Diagnostics," *Advanced Materials* 30, no. 41 (2018): 1800444, https://doi.org/10.1002/ADMA.201800444.

25. R. K. Misra, S. Aharon, B. Li, et al., "Temperature- and Component-Dependent Degradation of Perovskite Photovoltaic Materials under Concentrated Sunlight," *Journal of Physical Chemistry Letters* 6, no. 3 (2015): 326–330, https://doi.org/10.1021/JZ502642B/SUPPL_FILE/JZ502642B_SI_001.PDF.

26. R. Guo, M. V. Khenkin, G. E. Arnaoutakis, et al., "Initial Stages of Photodegradation of $MAPbI_3$ Perovskite: Accelerated Aging with Concentrated Sunlight," *Solar RRL* 4, no. 2 (2020): 1900270, https://doi.org/10.1002/SOLR.201900270.

27. R. Gottesman, L. Gouda, B. S. Kalanoor et al., "Photoinduced Reversible Structural Transformations in Free-Standing $CH_3NH_3PbI_3$ Perovskite Films," *Journal of Physical Chemistry Letters* 6, no. 12 (2015): 2332–2338, https://doi.org/10.1021/ACS.JPCLETT.5B00994/SUPPL_FILE/JZ5B00994_SI_001.PDF.

28. W. A. Quitsch, L. Gouda, B. S. Kalanoor et al., "The Role of Excitation Energy in Photobrightening and Photodegradation of Halide Perovskite Thin Films," *Journal of Physical Chemistry Letters* 9, no. 8 (2018): 2062–2069, https://doi.org/10.1021/ACS.JPCLETT.8B00212/ASSET/IMAGES/LARGE/JZ-2018-00212E_0002.JPEG.

29. T. A. Berhe, J.-H. Cheng, W.-N. Su, et al., "Identification of the Physical Origin behind Disorder, Heterogeneity, and Reconstruction and Their Correlation with the Photoluminescence Lifetime in Hybrid Perovskite Thin Films," *Journal of Materials Chemistry A* 5, no. 39 (2017): 21002–21015, https://doi.org/10.1039/C7TA04615D.

30. L. Liu, L. Deng, S. Huang, et al., "Photodegradation of Organometal Hybrid Perovskite Nanocrystals: Clarifying the Role of Oxygen by Single-Dot Photoluminescence," *Journal of Physical Chemistry Letters* 10, no. 4 (2019): 864–869, https://doi.org/10.1021/ACS.JPCLETT.9B00143/ASSET/IMAGES/LARGE/JZ-2019-001436_0004.JPEG.

31. R. K. Misra, L. Ciammaruchi, S. Aharon, et al., "Effect of Halide Composition on the Photochemical Stability of Perovskite Photovoltaic Materials," *ChemSusChem* 9, no. 18 (2016): 2572–2577, https://doi.org/10.1002/cssc.201600679.

32. Q. C. Burlingame, Y.-L. Loo, and E. A. Katz, "Accelerated Ageing of Organic and Perovskite Photovoltaics," *Nature Energy* 8 (2023): 1300–1302, https://doi.org/10.1038/s41560-023-01330-8.

33. A. K. M., M. V. Khenkin, F. Di Giacomo, et al., "Bias-Dependent Stability of Perovskite Solar Cells Studied Using Natural and Concentrated Sunlight," *Solar RRL* 4, no. 2 (2020): 1900335, https://doi.org/10.1002/SOLR.201900335.

34. J. M. Gordon, D. Babai, and D. Feuermann, "A High-Irradiance Solar Furnace for Photovoltaic Characterization and Nanomaterial Synthesis," *Solar Energy Materials and Solar Cells* 95, no. 3 (2011): 951–956, https://doi.org/10.1016/J.SOLMAT.2010.11.030.

35. A. Braun, B. Hirsch, A. Vossier, E. A. Katz, and J. M. Gordon, "Temperature Dynamics of Multijunction Concentrator Solar Cells up to Ultra-High Irradiance," *Progress in Photovoltaics: Research and Applications* 21, no. 2 (2013): 202–208, https://doi.org/10.1002/PIP.1179.

36. G. E. Arnaoutakis, N. Samoylova, M. V. Khenkin, R. Guo, and E. A. Katz, "*In-Situ Photoluminescence Kinetics of Lead Halide Perovskites Under Sunlight Excitation*,"*2019* Conference on Lasers and Electro-Optics Europe and European Quantum Electronics Conference CLEO/Europe-EQEC, 2019, p. 2019, https://doi.org/10.1109/CLEOE-EQEC.2019.8872642.

37. N. Kataoka, Y. Shima, K. Nakajima, and K. Nakamura, "Triple-Halide Wide-Band Gap Perovskites with Suppressed Phase Segregation for Efficient Tandems," *Science* 367, no. 6482 (2020): 1097–1112, https://doi.org/10.1126/SCIENCE.AAZ4639.

38. B. J. Foley, D. L. Marlowe, K. Sun et al., "Temperature Dependent Energy Levels of Methylammonium Lead Iodide Perovskite," *Applied Physics Letters* 106, no. 24 (2015): 581–586, https://doi.org/10.1063/1.4922804/27521.

39. W. L. Leong, Z-En Ooi, D. Sabba, et al., "Identifying Fundamental Limitations in Halide Perovskite Solar Cells," *Advanced Materials* 28, no. 12 (2016): 2439–2445, https://doi.org/10.1002/adma.201505480.

40. W. A. Saidi, S. Poncé, and B. Monserrat, "Temperature Dependence of the Energy Levels of Methylammonium Lead Iodide Perovskite from First-Principles," *Journal of Physical Chemistry Letters* 7, no. 24 (2016): 5247–5252, https://doi.org/10.1021/ACS.JPCLETT.6B02560.

41. A. M. Stoneham, *Theory of Defects in Solids: Electronic Structure of Defects in Insulators and Semiconductors* (Oxford University Press, 2001).

42. J. Friedel, "Solid State Physics. Volume 5," *Journal of Physics and Chemistry of Solids* 5, no. 3 (1958): 236, https://doi.org/10.1016/0022-3697(58)90073-8.

43. M. A. Reshchikov, "Temperature Dependence of Defect-Related Photoluminescence in III-V and II-VI Semiconductors," *Journal of*

Applied Physics 115, no. 1 (2014), https://doi.org/10.1063/1.4838038/139068.

44. D. Hong, Y. Zhou, S. Wan, X. Hu, D. Xie, and Y. Tian, "Nature of Photoinduced Quenching Traps in Methylammonium Lead Triiodide Perovskite Revealed by Reversible Photoluminescence Decline," *ACS Photonics* 5, no. 5 (2018): 2034–2043, https://doi.org/10.1021/ACSPHOTONICS.7B01537/ASSET/IMAGES/LARGE/PH-2017-01537P_0007.JPEG.

45. H. Yuan, E. Debroye, G. Caliandro, et al., "Photoluminescence Blinking of Single-Crystal Methylammonium Lead Iodide Perovskite Nanorods Induced by Surface Traps," *ACS Omega* 1, no. 1 (2016): 148–159, https://doi.org/10.1021/ACSOMEGA.6B00107/ASSET/IMAGES/LARGE/AO-2016-00107D_0006.JPEG.

46. Y. Tian, A. Merdasa, E. Unger et al., "Enhanced Organo-Metal Halide Perovskite Photoluminescence from Nanosized Defect-Free Crystallites and Emitting Sites," *Journal of Physical Chemistry Letters* 6, no. 20 (2015): 4171–4177, https://doi.org/10.1021/ACS.JPCLETT.5B02033/SUPPL_FILE/JZ5B02033_SI_001.PDF.

47. G. Yuan, C. Ritchie, M. Ritter, S. Murphy, D. E. Gómez, and P. Mulvaney, "The Degradation and Blinking of Single $CsPbI_3$ Perovskite Quantum Dots," *Journal of Physical Chemistry C* 122, no. 25 (2018): 13407–13415, https://doi.org/10.1021/ACS.JPCC.7B11168/ASSET/IMAGES/MEDIUM/JP-2017-111689_M010.GIF.

48. X. Wang, Z. Jiao, H. Fang et al., "Specific Influences of Trap States with Distinct Spatial and Energetic Distributions on Ion Migration Dynamics in Metal Halide Perovskites," *Nano Letters* 22 (2024): 49, https://doi.org/10.1021/ACS.NANOLETT.4C05700/ASSET/IMAGES/LARGE/NL4C05700_0005.JPEG.

49. E. T. Hoke, D. J. Slotcavage, E. R. Dohner, A. R. Bowring, H. I. Karunadasa, and M. D. McGehee, "Reversible Photo-Induced Trap Formation in Mixed-Halide Hybrid Perovskites for Photovoltaics," *Chemical Science* 6, no. 1 (2015): 613–617, https://doi.org/10.1039/C4SC03141E.

50. K. Suchan, A. Merdasa, C. Rehermann, E. L. Unger, and I. G. Scheblykin, "Complex Evolution of Photoluminescence during Phase Segregation of MAPb(I1-xBrx)3 Mixed Halide Perovskite," *Journal of Luminescence* 221 (2020): 117073, https://doi.org/10.1016/j.jlumin.2020.117073.

51. S. Fang, W. Yao, Z. Hu, et al., "Stability in Photoinduced Instability in Mixed-Halide Perovskite Materials and Solar Cells," *Journal of Physical Chemistry C* 125, no. 39 (2021): 21370–21380, https://doi.org/10.1021/acs.jpcc.1c07620.

52. D. V. Athapaththu, M. E. Kordesch, and J. Chen, "Monitoring Phase Separation and Dark Recovery in Mixed Halide Perovskite Clusters and Single Crystals Using In Situ Spectromicroscopy," *Journal of Physical Chemistry Letters* 15, no. 4 (2024): 1105–1111, https://doi.org/10.1021/acs.jpclett.3c03280.

53. A. J. Barker, A. Sadhanala, F. Deschler, et al., "Defect-Assisted Photoinduced Halide Segregation in Mixed-Halide Perovskite Thin Films," *ACS Energy Letters* 2, no. 6 (2017): 1416–1424, https://doi.org/10.1021/acsenergylett.7b00282.

54. C. Dreessen and P. Daniel, "Radiative and Non-Radiative Losses by Voltage-Dependent in-Situ Photoluminescence in Perovskite Solar Cell Current-Voltage Curves," *Journal of Luminescence* 222, no. 2020 (2019): 112117.

55. C. Dreessen, L. Gil-Escrig, M. Hülsbeck, M. Sessolo, H. J. Bolink, and T. Kirchartz, "Effective Steady-State Recombination Decay Times in Comparison to Time-Resolved Photoluminescence Decay Times in Halide Perovskite Solar Cells," *Solar RRL* 8, no. 23 (2024): 2400504, https://doi.org/10.1002/SOLR.202400504.

56. A. D. Bui, N. Mozaffari, T. N. Truong, et al., "*Electrical Properties of Perovskite Solar Cells by Illumination Intensity and Temperature-Dependent Photoluminescence Imaging, Progress in Photovoltaics: Research and Applications*30 (2022): 1038, https://doi.org/10.1002/PIP.3498.

57. S. Akel, Y. Wang, G. Yan, U. Rau, and T. Kirchartz, "Charge Carrier Collection Losses in Lead-Halide Perovskite Solar Cells," *Advanced Energy Materials* 14, no. 47 (2024): 2401800, https://doi.org/10.1002/AENM.202401800.

58. G. E. Arnaoutakis, D. Busko, B. S. Richards, A. Ivaturi, J. M. Gordon, and E. A. Katz, "Ultra-Broadband Near-Infrared Upconversion for Solar Energy Harvesting," *Solar Energy Materials and Solar Cells* 269 (2024): 112783, https://doi.org/10.1016/J.SOLMAT.2024.112783.

59. E. A. Katz, D. Faiman, S. M. Tuladhar, et al., "Temperature Dependence for the Photovoltaic Device Parameters of Polymer-Fullerene Solar Cells under Operating Conditions," *Journal of Applied Physics* 90, no. 10 (2001): 5343–5350, https://doi.org/10.1063/1.1412270.

Supporting Information

Additional supporting information can be found online in the Supporting Information section.